Environmental Science and Ecotechnology 21 (2024) 100421

Contents lists available at ScienceDirect

Environmental Science and Ecotechnology

journal homepage: www.journals.elsevier.com/environmental-science-and-ecotechnology/

Original Research

Overlooked interaction between redox-mediator and bisphenol-A in permanganate oxidation

Honglong Zhang [a, b], Qiaoqiao Zhao [c], Kangbao Zhong [c], Ruopeng Bai [c], Jiaojiao Dong [d], Jun Ma [a], Jing Zhang [a, *], Timothy J. Strathmann [e]

[a] School of Environment, Harbin Institute of Technology, Harbin, 150090, PR China
[b] Institute of Nuclear and New Energy Technology, Tsinghua University, Beijing, 100084, PR China
[c] School of Chemistry and Chemical Engineering, Chongqing Key Laboratory of Chemical Theory and Mechanism, Chongqing University, Chongqing, 401331, PR China
[d] College of Environment and Ecology, Chongqing University, Chongqing, 400045, PR China
[e] Department of Civil and Environmental Engineering, Colorado School of Mines, 1500 Illinois Street, Golden, CO, 80401, United States

ARTICLE INFO

Article history:
Received 21 September 2023
Received in revised form
13 April 2024
Accepted 14 April 2024

Keywords:
Permanganate
Redox-mediator
Bisphenol-A
Radical cross-coupling
Complexation

ABSTRACT

Research efforts on permanganate (Mn(VII)) combined with redox-mediator (RM), have received increasing attention due to their significant performance for bisphenol-A (BPA) removal. However, the mechanisms underpinning BPA degradation remain underexplored. Here we show the overlooked interactions between RM and BPA during permanganate oxidation by introducing an RM—N-hydroxyphthalimide (NHPI). We discovered that the concurrent generation of MnO_2 and phthalimide-*N*-oxyl (PINO) radical significantly enhances BPA oxidation within the pH range of 5.0–6.0. The detection of radical cross-coupling products between PINO radicals and BPA or its derivatives corroborates the pivotal role of radical cross-coupling in BPA oxidation. Intriguingly, we observed the formation of an NHPI-BPA complex, which undergoes preferential oxidation by Mn(VII), marked by the emergence of an electron-rich domain in NHPI. These findings unveil the underlying mechanisms in the Mn(VII)/RM system and bridge the knowledge gap concerning BPA transformation via complexation. This research paves the way for further exploration into optimizing complexation sites and RM dosage, significantly enhancing the system's efficiency in water treatment applications.

1. Introduction

As one of the endocrine-disrupting chemicals (EDCs) [1–3], bisphenol-A (BPA, a typical EDC) has been widely detected in various aquatic environments with concentrations from ng L^{-1} to μg L^{-1} [4–6]. Moreover, BPA cannot be removed efficiently in conventional water treatment processes [7]. This necessitates the development of effective BPA removal technologies, with chemical oxidation being a promising approach [8,9]. Mn(VII) is an effective and environmentally friendly oxidant widely used for its stability, ease of handling, relatively low cost, and no generation of by-products after oxidation [10,11]. However, compared with ozonation, Fenton, and other advanced oxidation processes, the reaction rate of organic contaminants (such as BPA) with Mn(VII) is relatively low [12–14].

Recently, it has been reported that redox-mediators (RMs) (e.g., 1-hydroxybenzotriazole (HBT) [11,15], 2,2,6,6-tetramethylpiperidine-*N*-oxyl (TEMPO) [13,16], 9-azabicyclo[3.3.1]nonane *N*-oxyl (ABNO) [17], and 2-phenyl-4,4,5,5-tetramethylimidazoline-3-oxide-1-oxyl (PTIO) [18]) act as catalysts or electron shuttles for transferring electrons between BPA and Mn(VII). In these systems, HBT, TEMPO, ABNO, and PTIO are converted to their higher valent states (i.e., $HBT^{\bullet}$, $TEMPO^{+}$, $ABNO^{+}$, and $PTIO^{+}$) following a reaction with Mn(VII), and then BPA is degraded rapidly following three distinct degradation pathways, namely, hydroxylation, β-scission, and radical cross-coupling [11,13], among which hydroxylation predominates according to the previous results [11,13]. Radical cross-coupling is the unique pathway observed only in the Mn(VII)/RMs systems, in contrast to observations reported for other oxidation systems (e.g., ozone [19], ferrate [20], Mn(VII) [21],

* Corresponding author.
E-mail address: zhang_jing@hit.edu.cn (J. Zhang).

https://doi.org/10.1016/j.ese.2024.100421

and Mn(VII)/Ru(III) [22]). Thus, we speculated that some interactions between the RM and BPA might be overlooked during reactions involving Mn(VII) [11,13].

There are several binding interactions between dissolved organic matter (DOM) and BPA, such as hydrogen bonds, aromatic stacking, hydrophobic weak forces, and electrostatic interactions [23,24]. In 2012, Zhu et al. proposed that the hydrogen bond of the DOM-BPA complex is preferred over their aromatic interactions based on density-functional theory (DFT) calculation [23]. In 2022, Hu's group demonstrated that π−π interaction of the aromatic structure of humic acids (HA, a primary component of DOM) with the aromatic structure of BPA resulted in forming a polar complex [25]. This π−π interaction resulted in more electrons transferring to the carbonyl group in the benzoquinone of HA, producing electron-rich phenolic −OH groups in this complex. An electron-poor area on BPA's aromatic rings facilitates its preferential removal [25]. Similar to DOM (or HA), many RMs possess aromatic structures that might interact with BPA via π−π interaction to form the complex. However, the possible complexation between RM and BPA has not yet been considered in the Mn(VII)/RM system.

Generally, RMs include nitroxides-RMs (e.g., *N*-hydroxyphthalimide (NHPI), HBT, TEMPO, ABNO, and PTIO) and phenoxides-RMs [11,17,18]. It has been proved the capacity of electron transfer from nitroxides-RMs is stronger than that of phenoxides-RMs [11]. Among these nitroxides-RMs, HBT, as an electron shuttle, efficiently enhanced the reaction between Mn(VII) and BPA but itself was also degraded by Mn(VII) [11]. Conversely, TEMPO, ABNO, and PTIO can serve as catalysts due to their cyclic transformation of >N−O•, >N−OH, and >N$^+$=O [13,17,18], realizing the cycle work for enhancing BPA decay with little loss in Mn(VII) solution. The toxicity of TEMPO, ABNO, and PTIO hinders their application in real aquatic environments. NHPI with lower toxicity has a similar cyclic transformation to TEMPO (Scheme 1) [26,27]. Besides, NHPI can be easily loaded onto heterogeneous materials (e.g., metal-organic frameworks, porous polymers, and high-surface-area carbons) [28]; thus, it might be superior to the reported nitroxides-RMs (i.e., HBT [11], TEMPO [13], ABNO [17], and PTIO [18]). Subsequently, NHPI was chosen as a new redox mediator in this study.

In our study of the Mn(VII)/NHPI system, we began by evaluating the impacts of NHPI dosage and solution pH on the oxidation kinetics of BPA, then identified the involved reactive species, proposed the mechanism, and highlighted the radical cross-coupling pathway's contribution to BPA oxidation enhancement. Lastly, we investigated the complexation effect of RM in enhancing BPA oxidation by Mn(VII).

2. Materials and methods

2.1. Chemicals and reagents

Potassium permanganate (Mn(VII)), bisphenol-A (BPA), *N*-hydroxy phthalimide (NHPI), 2,2,6,6-tetramethylpiperidine-*N*-oxyl (TEMPO), syringaldehyde (SYD), humic acid (HA), 2,6-di-*tert*-butylphenol, and hexafluoroisopropanol were obtained from Aladdin (Shanghai, China). Methyl phenyl sulfoxide (PMSO) and methyl phenyl sulfone ($PMSO_2$) were purchased from TCI (Shanghai, China). Methanol, acetonitrile, and acetic acid of high-performance liquid chromatography (HPLC) grade were supplied by Merck (Darmstadt, Germany). All other reagents and solvents were from Sinopharm Chemical Reagent Co., Ltd. (Shanghai, China). All solutions were prepared using deionized water from a Millipore water purification system.

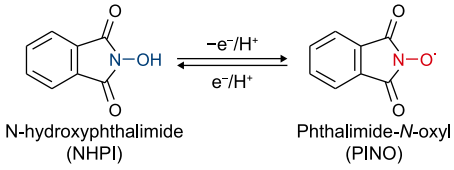

Scheme 1. Cyclic transformation of NHPI and PINO.

2.2. Experimental procedures

All experiments were conducted in amber glass bottles continuously mixed by magnetic stirring and maintained at 25 ± 1 °C by a circulating water jacket. Batch reactions were initiated by adding Mn(VII) or colloidal MnO_2 into solutions containing BPA or RM-BPA (i.e., the mixture of RM and BPA after 90 min mixing) at the desired concentration. A stable colloidal MnO_2 stock solution was prepared following our previous study [13]. The Mn(II) solution was prepared by mixing Mn(VII) and equivalent hydroxylamine under acidic conditions, and then a transparent solution was obtained. The pH of reaction solutions was controlled with acetate buffer (10 mM) for pH 5.0−6.0 and borate buffer (10 mM) for pH 7.0−9.0. It has been reported that acetate buffer and borate buffer had negligible effects on the Mn(VII)/redox-mediators system [11,13]. Samples were withdrawn at specified intervals, quenched with excess hydroxylamine (10 mM), and filtered before measuring residual organic compounds. All batch experiments were conducted in duplicate or triplicate, and uncertainties are presented as standard deviations.

2.3. Analytical methods

The concentration of BPA was determined by high-performance liquid chromatography (HPLC, Thermo Fisher Scientific UltiMate 3000) equipped with an XBridge BEH C18 column (5 μm, 4.6 × 150 mm) and a UV detector at wavelengths of 230 nm. The mobile phase consisted of acetonitrile and water (45:55, v/v) with a flow rate of 0.8 mL min^{-1}. Further details for analysis of PMSO and $PMSO_2$ are listed in Table S1. Transformation products of BPA were determined by liquid chromatography coupled to a tandem mass spectrometer (HPLC-MS/MS) (Thermo Fisher Scientific, USA). An XBridge BEH C18 column (5 μm, 4.6 × 150 mm) was used to separate products. The mobile phase consisted of 0.1% formic acid and acetonitrile, which increased linearly from 95/5 to 5/95 (water/acetonitrile) in the first 15 min and held for 4 min. The column temperature was kept constant at 45 °C. The flow rate was 0.4 mL min^{-1}. The HPLC effluent was diverted to the Q executive plus MS spectrometer by the diverter system. The mass spectra were recorded in the negative mode of ESI with the scan range of m/z = 50−750.

Electron paramagnetic resonance (EPR) spectroscopy spectra were obtained from EPR 200-Plus with continuous-wave X band frequency (Chinainstru& Quantumtech (Hefei) Co., Ltd.). Ultraviolet and visible (UV−vis) spectrophotometer (Persee Analytics TU-1901) was mainly used to record the decay of Mn(VII) and the continuous formation of MnO_2 in the range of 250−600 nm during reactions. The three-dimensional excitation-emission matrix (3D-EEM) fluorescence spectra of various samples (i.e., 500 μM RM, 50 μM BPA, and 500 μM RM after reaction with 50 μM BPA for desired mixing time in ultrapure water) were obtained on an F-7000 spectrometer (HITACHI) with a xenon excitation source. Slits were set to 5 nm for both excitation (Ex) and emission (Em).

2.4. Theoretical calculation

Density functional theory (DFT) calculation was performed using the Gaussian 16 program [29]. All geometry optimizations and

frequency calculations in this paper were performed with B3LYP functional [30] in implicit water at 6-31G(d,p) basis set, including solvation energy corrections and Grimme's D3 (BJ-damping) [31] dispersion corrections by using the Solvation Model Based on Density (SMD) [32] with the keyword in the Gaussian code route section "SCRF = (SMD, Solvent = water)". The frontier molecular orbital (FMO) analysis was generated using VMD [33] and Multiwfn [34].

The reaction free energy (ΔG) of the conversion of carbonyl groups of NHPI to form hydroxyl groups was calculated as $\Delta G = \Delta E + \Delta E_{ZPE} - T\Delta S + \Delta G_{pH}$, where ΔE is the difference of total energy, ΔE_{ZPE} and ΔS are the differences in the zero-point energy and the change of entropy, and T is the temperature (T = 298.15 K in this work). Since the reaction takes place in water, ΔG_{pH} is negligible.

3. Results and discussion

3.1. Oxidation kinetics of BPA in the Mn(VII)/NHPI system

The remarkable enhancement of BPA decay caused by NHPI was observed at pH 5.0 and 6.0 (Fig. 1a), suggesting NHPI is an effective redox-mediator for accelerating the oxidation of BPA by Mn(VII) under weakly acidic conditions. The pseudo-first-order reaction rate constant (k_{obs}, min^{-1}) for BPA in Mn(VII)/NHPI system increased from 0.04 to 0.34 min^{-1} as the NHPI dosage elevated from 0 μM to 50 μM (Fig. 1b). However, a further increase in the NHPI dosage resulted in a drop in the k_{obs} (Fig. 1; Fig. S1), owing to the self-quenching of excessive reactive intermediates [11,13,35].

The effect of pH on the removal of BPA (5 μM) was examined with a fixed concentration of Mn(VII) (50 μM) in the presence or absence of NHPI (0 and 50 μM). The k_{obs} of BPA removal by Mn(VII) alone climbed gradually from pH 5.0 to 9.0 (Fig. 1c) due to the oxidative rate of neutral BPA being lower than deprotonated BPA [16]. Observations also revealed that the k_{obs} of the Mn(VII)/NHPI system declined as the pH level rose from 5.0 to 7.0. However, it progressively increased over a pH range of 7.0–9.0. This can be attributed to (i) the pK_a value of NHPI being approximately 7.0 and (ii) the fraction of deprotonated BPA becoming dominant, with its first pK_a value at 9.2 [13]. Compared to Mn(VII) alone, NHPI enhanced BPA oxidation by Mn(VII) at pH 5.0–6.0 but lowered that at pH 7.0–9.0. This suggests that the direct Mn(VII) reactions with BPA outweigh the NHPI-driven pathway under neutral and alkaline conditions.

The pH-dependent profiles of k_{obs} (min^{-1}) in Mn(VII) combined with NHPI or HBT are of parabolic shape, while in the Mn(VII)/TEMPO and Mn(VII)/ABNO system, the k_{obs} (min^{-1}) rise with increasing pH (Fig. S2) [11,13,17]. In the Mn(VII) combined with TEMPO or ABNO systems, the reactive species $TEMPO^+$ or $ABNO^+$ can enhance organic contaminants removal over the wide pH range of 5.0–9.0 [13,16,17], but in the Mn(VII)/HBT system, the $HBT^•$ radical is only effective under acidic conditions [11]. This difference in pH-dependent profiles in these systems may be ascribed to the different properties of redox-mediators. In sum, the role of NHPI in Mn(VII) oxidation differed from that of TEMPO and ABNO, but it was similar to that of HBT. In the next section, we explored the mechanism of the Mn(VII)/NHPI system to elucidate the role of NHPI in detail.

3.2. Reactive species of Mn(VII)/NHPI system

Generally, the reactive species for BPA removal in the Mn(VII)/redox-mediators system includes Mn(VII) itself, *in situ* formed colloid MnO_2, and organic radicals or cations (e.g., $HBT^•$ [11], $TEMPO^+$ [13], and $ABNO^+$ [17]). Besides, there might be other intermediates of manganese, including Mn(VI), Mn(V), and Mn(III). However, considering their instability, their contribution to the reaction can be ignored unless in the presence of suitable ligands [11,36,37].

3.2.1. In situ formed colloidal MnO_2

Ultraviolet and visible spectrophotometry (UV–vis) scanning confirmed the *in situ* formation of colloidal MnO_2 with broad absorption from 300 to 430 nm when the Mn(VII) absorption at 526 nm decayed (Fig. S3). There is a good linear relationship between the absorbance at 418 and 526 nm (Fig. S4), suggesting the generation of *in situ* colloidal MnO_2 from the reduction of Mn(VII) [38,39]. According to the standard curve of MnO_2 (Fig. S5), it can be calculated that 30–50 μM colloidal MnO_2 was formed *in situ* when BPA was removed completely in the Mn(VII)/NHPI system (Fig. S3b). It has been reported that the removal of phenols by MnO_2 under acidic conditions is mainly via oxidation, with adsorption playing a minor role [39,40]. Besides, *in situ* formed MnO_2 could catalyze Mn(VII) oxidation of phenols [36]. Thus, the performance of BPA decay by colloidal MnO_2 should be investigated. The contribution of pre-synthesized colloidal MnO_2 on the oxidation of BPA at pH 5.0–6.0 is considerable (data at pH 7.0–9.0 not shown for negligible effect) (Fig. S6), indicating that *in situ* generated MnO_2 plays an important role in the removal of BPA in the Mn(VII)/NHPI system.

There was also an interaction between NHPI and *in situ* colloid MnO_2 at pH 5.0–6.0 (Fig. S7). The oxidation of BPA by colloid MnO_2/NHPI can be divided into two stages: fast and slow. In the fast stage (first 2 min), NHPI accelerated the oxidation of BPA by colloid MnO_2, indicating that other active species were generated (the detailed discussion was shown in 3.2.2). Then, the reaction tended

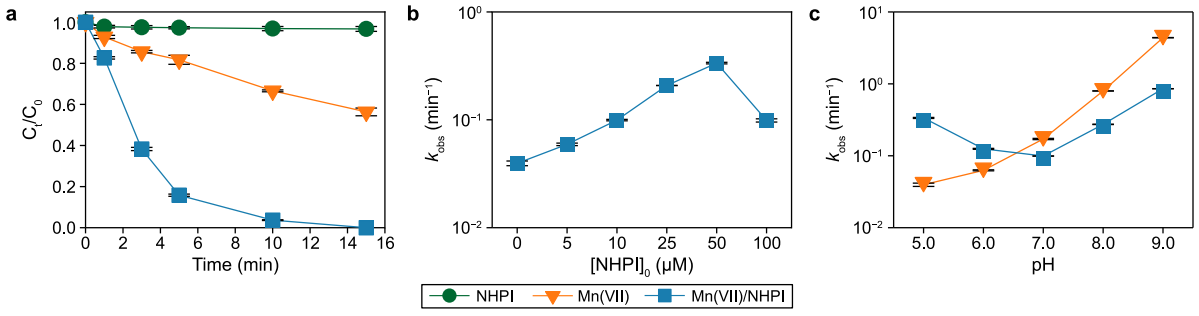

Fig. 1. **a**, Removal of BPA in NHPI, Mn(VII), and Mn(VII)/NHPI systems. **b**–**c**, Influence of NHPI dosage (**b**) and pH (**c**) on the pseudo-first-order reaction rate constant (k_{obs}, min^{-1}) of BPA oxidation by Mn(VII)/NHPI. Experimental conditions: $[Mn(VII)]_0$ = 50 μM (if any), $[BPA]_0$ = 5 μM, T = 25 ± 1 °C. For panel **a**, $[NHPI]_0$ = 50 μM, pH = 5.0; for panel **b**, $[NHPI]_0$ = 0–100 μM, pH = 5.0; for panel **c**, $[NHPI]_0$ = 50 μM, pH = 5.0–9.0.

to be stagnant, implying the complete consumption of colloid MnO_2 by massive NHPI in the slow stage.

3.2.2. *In situ* formed PINO radical

Manganese species could convert methyl phenyl sulfoxide (PMSO) to methyl phenyl sulfone ($PMSO_2$) (equations (1)–(3)) [11,41], while some radicals (e.g., $HBT^{\bullet}$ radical [11], hydroxyl radical [13], and sulfate radical [11]) result in hydroxylated and/or polymeric products. PMSO was converted entirely to $PMSO_2$ in Mn(VII) solution (Fig. S8). However, the formation of $PMSO_2$ decreased to ~86% in the Mn(VII)/NHPI system. At a retention time of 4.5 min in the HPLC spectra, a new product was detected (Fig. S9), suggesting the involvement of some radicals in the Mn(VII)/NHPI system.

$$Mn(VII) + PMSO \rightarrow Mn(V) + PMSO_2 \quad (1)$$

$$Mn(V) + PMSO \rightarrow Mn(III) + PMSO_2 \quad (2)$$

$$2Mn(III) \rightarrow Mn(II) + Mn(IV) \quad (3)$$

Hydroxyl radical was yielded from the Mn(VII)/humic-acid system under oxygen saturation conditions [42]; thus, we also tested the presence of hydroxyl radical in the Mn(VII)/NHPI system. As one of the effective scavengers of hydroxyl radicals, methanol can trap hydroxyl radicals at high speed ($>1.2 \times 10^9$ M^{-1} s^{-1}) [13,43]. However, methanol hardly affected the removal of BPA in the Mn(VII)/NHPI system (Fig. S10). Therefore, the existence of hydroxyl radicals can be excluded in the Mn(VII)/NHPI system.

As depicted in Scheme 1, NHPI was converted to phthalimide-*N*-oxyl (PINO radical) via one-electron transfer, and Mn(VII) served as the one-electron capturer. D'Alfonso et al. reported that antioxidants (generally a series of phenolic compounds, such as 2,2,5,7,8-pentamethylchroman-6-ol, 2,6-di-*tert*-butyl-4-substituted phenols, and 2,6-dimethyl-4-substituted phenols) could efficiently quench PINO [44]. Hence, we introduced the 2,6-di-*tert*-butylphenol into the Mn(VII)/NHPI systems and found that it significantly inhibited the removal of BPA (Fig. S10). Besides, BPA removal was more efficient with Mn(VII)/2,6-di-*tert*-butylphenol than the Mn(VII)/NHPI/2,6-di-*tert*-butylphenol system, suggesting the formation and essential role of PINO (Fig. S10). Consequently, the new product of PMSO (Fig. S9) may be generated in the reaction between PINO radical and PMSO. Moreover, the reduction potential of PINO decreases with climbing pH, and PINO can not be formed or exist at pH > 7.2 due to its instability [45]. At pH > 7.2, NHPI mainly competes with BPA for Mn(VII). Therefore, the high consumption of Mn(VII) by NHPI caused the inhibition of BPA decay under alkaline conditions (Fig. 1c).

In previous studies, UV–vis scanning, electron paramagnetic resonance (EPR) spectroscopy, and flash photolysis were used to verify the presence of the PINO radical [46,47]. Among these techniques, UV–vis spectroscopy is the most feasible. Thus, we monitored the UV–vis spectrum of the mixture of Mn(VII) and NHPI and found that 1 mM Mn(VII) was entirely reduced to Mn(II) by 1 mM NHPI, with the color of the solution changing from purple to transparent (Fig. S11). The increased absorbance in the 350–400 nm range can be assigned to forming the PINO radical (Fig. 2; Fig. S12), since the weak absorbance of the equivalent NHPI and Mn(II). The broad absorption from 300 to 430 nm of MnO_2 (Fig. S3) also included the faint absorbance of the PINO radical. We also applied EPR to confirm the presence of the PINO radical. However, the strong signals of Mn(II) cover the signal of the PINO radical (Fig. S13). Notably, the reactivity of Mn(VII) and *in situ* formed colloidal MnO_2 might be affected by Mn(II) [48,49], since much Mn(II) would be generated in the Mn(VII)/NHPI system.

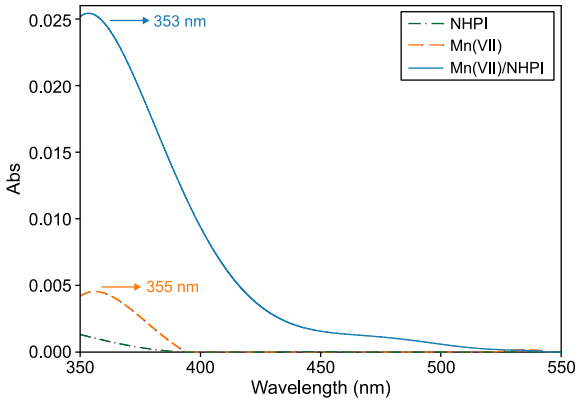

Fig. 2. UV–vis spectra of Mn(VII)/NHPI mixture, NHPI, and Mn(II) in acetic acid. Experimental conditions: $[Mn(VII)]_0 = 1$ mM, $[NHPI]_0 = 1$ mM, $[Mn(II)]_0 = 1$ mM, T = 25 ± 1 °C, pH = 2.7, reaction time = 30 s.

To further prove the existence of the PINO radical, the transformation products of BPA were detected using HPLC-MS/MS with full scan mode. Fig. 3 presents BPA itself and three important transformation products (all transformation products in Table S2 and the corresponding ion mass spectra of other transformation products in Fig. S14). PINO-BPA with the molecular ions of $m/z = 388$ ($[M - H]^- = 388$) was identified as a coupling product between PINO and BPA. Similarly, the PINO-BPA-OH ($m/z = 404$) was the coupling product between PINO and hydroxylated BPA (BPA-OH, $m/z = 243$). Hence, the transformation products revealed the interaction between the PINO radical and BPA or its products and also confirmed the formation of the PINO radical.

3.3. Proposed mechanism of Mn(VII)/NHPI system

In sum, the Mn(VII)/NHPI system involves multiple oxidizing species being active for BPA removal, such as Mn(VII) itself [21], *in situ* formed MnO_2 (reduction product of Mn(VII)) [50], and PINO radical (a product of the reaction between Mn(VII) and NHPI) [47,51]. As illustrated in Scheme 2, NHPI was preferentially oxidized by Mn(VII) via a reversible electron transfer to the PINO radical, which was responsible for the acceleration of BPA oxidation by hydrogen attraction. Then, $BPA^{\bullet}$ was formed and cross-coupled with PINO to generate PINO-BPA. At the same time, colloid MnO_2 was generated from the reduction of Mn(VII), which could also oxidize BPA under acidic conditions. Besides, the accelerated oxidation of BPA by colloid MnO_2 in the presence of NHPI was obtained at pH 5.0–6.0 (Fig. S7), suggesting that PINO could also be produced from the reaction between NHPI and colloid MnO_2. BPA-OH produced via the reaction of BPA and Mn(VII) (or *in situ* colloid MnO_2) was transformed to PINO-BPA-OH by cross-coupling between PINO and BPA-OH.

BPA decay included three pathways: hydroxylation, β-scission, and PINO cross-coupling (Fig. 4). Notably, BPA and several transformation products from hydroxylation and β-scission cross-coupled with PINO, resulting in considerable PINO cross-coupling products (i.e., TP5–TP10) (Table S2; Figs. 3 and 4; Fig. S14), indicating the cross-coupling pathway caused by PINO radical could not be ignored in the Mn(VII)/NHPI system.

3.4. Complexation between RMs and BPA

Humic acid (HA) interacted with the aromatic structure of BPA

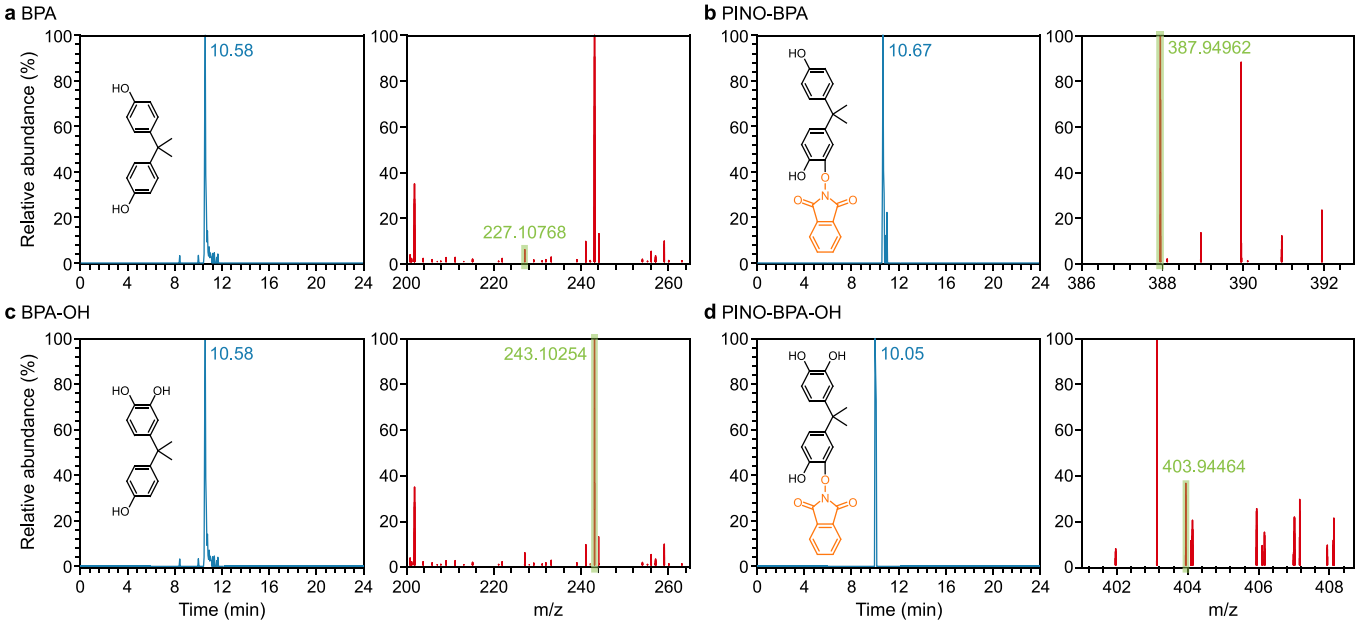

Fig. 3. HPLC-MS/MS full-scan chromatograms of the solution containing BPA and Mn(VII) in the presence of NHPI and the corresponding ion mass spectra of BPA (**a**) and three products, PINO-BPA (**b**), BPA-OH (**c**), and PINO-BPA-OH (**d**).

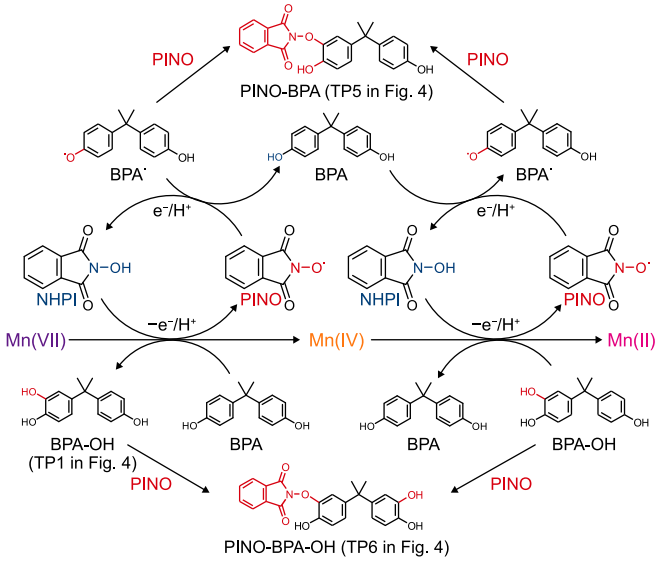

Scheme 2. Proposed mechanism of oxidation of BPA by Mn(VII) in the presence of NHPI.

via π−π conjugation, forming the π-conjugated HA-BPA complex, which could be monitored by three-dimensional excitation-emission matrix fluorescence spectroscopy (3D-EEM) [25]. Similar to HA, RMs (such as NHPI, TEMPO, and syringaldehyde (SYD)) [11,17] are also redox-active organics, possibly resulting in binding interaction between RMs and BPA. It may reveal an unrecognized role of RMs.

The characteristic fluorescence peak A of BPA decreased after interaction with NHPI instantly, and its characteristic peak B disappeared at the same time (Fig. 5), ascribed to the possible blocking effect of NHPI for BPA in the early stage of mixing (i.e., mixing NHPI and BPA for 0−30 min). The emergence of a new peak (Peak C) in the NHPI-BPA mixture, indicative of a humic acid-like fluorescent

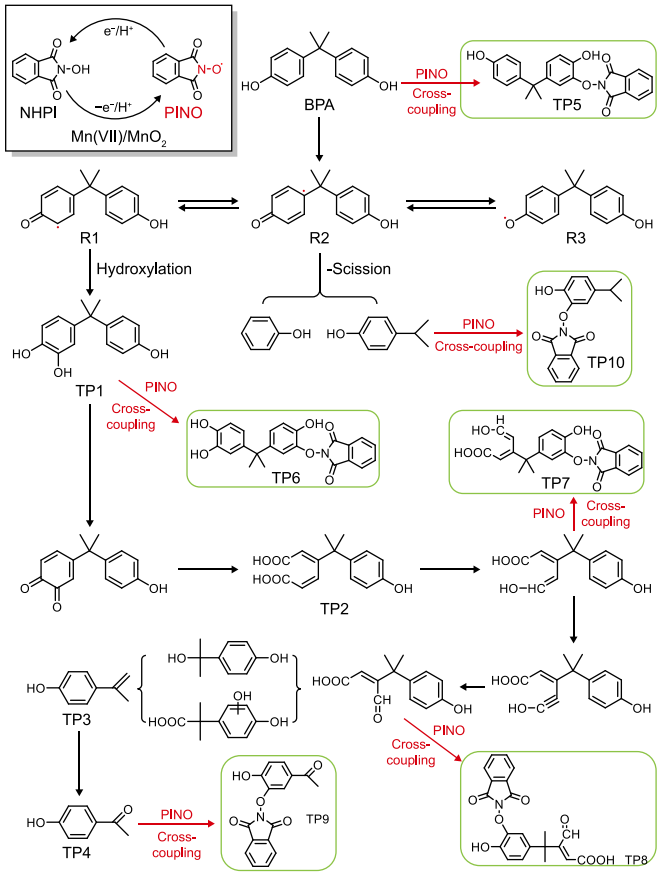

Fig. 4. Proposed reaction pathways of BPA in the Mn(VII)/NHPI system. BPA and TP1−TP10 were detected, and other transformation products were proposed.

substance [52,53], after 60−90 min of mixing (Fig. 5), confirmed the NHPI-BPA complex formation. UV−vis spectra confirmed the

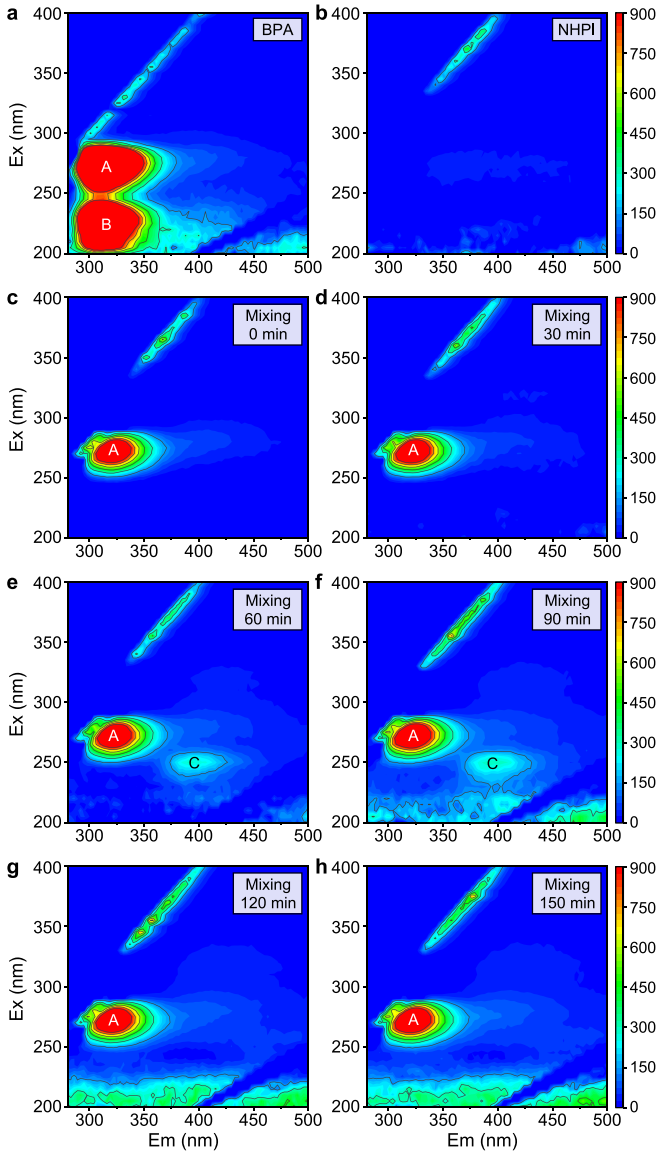

Fig. 5. **a**–**b**, 3D-EEM fluorescence spectroscopy of BPA (**a**) and NHPI (**b**). **c**–**h**, 3D-EEM fluorescence spectroscopy of BPA after mixing with NHPI for 0 min (**c**), 30 min (**d**), 60 min (**e**), 90 min (**f**), 120 min (**g**), and 150 min (**h**) in ultrapure water. Experimental conditions: $[NHPI]_0$ = 500 μM, $[BPA]_0$ = 50 μM, T = 25 ± 1 °C.

complexation between NHPI and BPA at 90 min (Fig. S15). Interestingly, NHPI-BPA decomplexation occurred when the mixing time extended to 120–150 min (Fig. 5). Thus, an optimal 90-min mixing time was established for forming an integral NHPI-BPA complex and used in subsequent experiments.

To explore the role of complexation and interaction between NHPI and BPA, we conducted batch experiments with the NHPI and BPA mixed for 90 min, and then the Mn(VII) was dosed to initiate the reaction, namely the complexed BPA decay in Mn(VII) (a legend in Fig. 6). The control group was also conducted under the same reaction condition with NHPI and BPA dosed into the Mn(VII) solution together, namely the uncomplexed BPA decay in Mn(VII) (legend in Fig. 6). Compared with uncomplexed BPA, the degradation of complexed BPA was faster (Fig. 6). The same preferential degradation of complexed BPA than its uncomplexed counterparts was also observed in the TEMPO-, SYD-, and HA-enhanced Mn(VII) oxidation systems (Fig. S16), which means the complexed BPA was

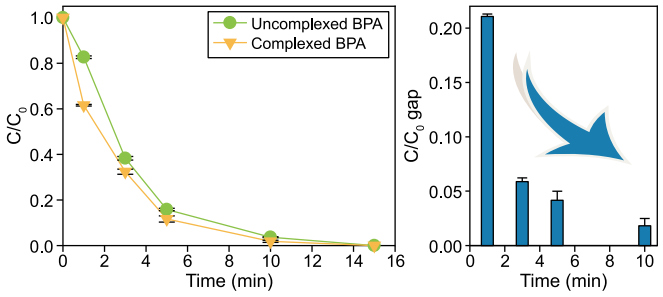

Fig. 6. Oxidation kinetics of uncomplexed BPA and complexed BPA by Mn(VII)/NHPI. The right side shows the C/C_0 gap between uncomplexed BPA and complexed BPA. Experimental conditions: $[Mn(VII)]_0$ = 50 μM, $[BPA]_0$ = 5 μM, $[NHPI]_0$ = 50 μM, pH = 5.0, T = 25 ± 1 °C, mixing time for complexed BPA = 90 min.

removed preferentially in the Mn(VII) solution. There was a commonality among several types of RMs.

Overall, the preferential removal of complexed BPA was obtained in the Mn(VII) solution within an initial 2 min (Fig. 6), which might be ascribed to the sufficient complexation at 90 min mixing (Fig. 5). As the reaction proceeded, the removal difference between uncomplexed and complexed BPA became small (Fig. 6), which might be related to the decomplexation of NHPI-BPA after 90 min (Fig. 5). We also compared the removal of uncomplexed BPA with the complexed BPA with TEMPO, SYD, and HA. We found that all the BPA pre-mixed with those RMs were degraded more rapidly at the beginning stage of reactions (Fig. S16), similar to the NHPI-based system.

A previous report has verified the HA-BPA complex consists of an electron-rich area and an electron-poor area, and the uneven distribution of electron clouds promoted the degradation of BPA [25]. Similar to the HA-BPA complex, the NHPI-BPA electron-donor-acceptor complex could also be optimized by DFT calculations. BPA could interact with NHPI by both hydrogen bonds and π–π electrostatic forces between their aromatic rings in the electron-donor-acceptor complex (Fig. 7a). An adsorption energy of −1.09 eV was found, enabling subsequent charge transfer. Orbital analysis (Fig. 7b) showed that the highest occupied molecular orbital (HOMO) was located in BPA, while the lowest unoccupied molecular orbital (LUMO) was located in NHPI, indicating that electrons transfer from HOMO (BPA fragment) to LUMO (NHPI fragment) occurring in the electron-donor-acceptor complex. As a result, the charge of NHPI moiety changes to −0.002 e after BPA is adsorbed, confirming the electron transfer from the aromatic rings of BPA to that of NHPI in the complex. In addition, the surface electrostatic potential of electron-donor-acceptor (Fig. 7c) indicated that NHPI was electron-rich; therefore, oxidation of the electron-donor-acceptor complex by Mn(VII) occurred on NHPI moiety. This explains why the addition of NHPI could accelerate the oxidation of BPA.

4. Conclusion

The removal and degradation mechanism of BPA by the Mn(VII) combined with NHPI (a typical RM) system were thoroughly elucidated. Crucially, this study unveiled, for the first time, the previously overlooked interaction between sufficient RM and BPA in the Mn(VII) solution. Compared with the Mn(VII) alone system, combining Mn(VII) and NHPI improved the removal of BPA under weakly acidic conditions. The effect of NHPI dosage and initial pH on the oxidation of BPA by Mn(VII)/NHPI was examined. The pseudo-first-order reaction rate constant (k_{obs}) increased linearly as the NHPI dosage increased from 0 to 50 μM. The k_{obs} decreased

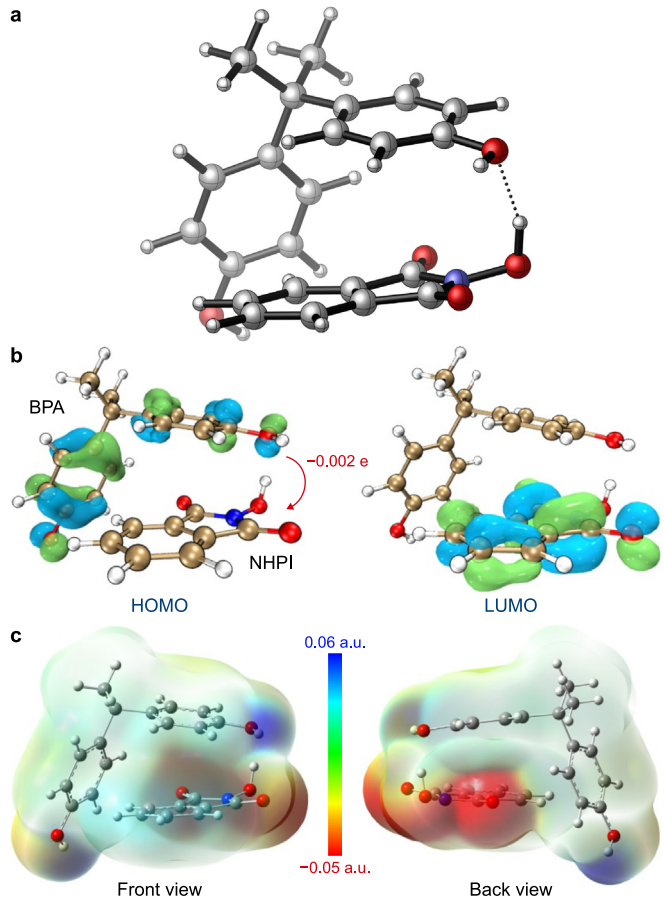

Fig. 7. a, Optimum configuration of NHPI-BPA complex with the lowest energy. **b**, HOMO and LUMO for BPA on the NHPI model fragments with an iso-value of 0.02. **c**, Surface electrostatic potential of NHPI-BPA complex. The blue area prefers adopting electrons, and the red area prefers donating electrons.

with pH climbing at pH 5.0–7.0, attributing to the decreased reactivity of *in situ* formed MnO_2 and instability of PINO radical as pH increases. The mechanism of the Mn(VII)/NHPI system was proposed. *In situ* PINO radical was formed from the electron transfer between manganese species (i.e., Mn(VII) and *in situ* formed MnO_2) and NHPI, which was responsible for accelerating BPA oxidation via hydrogen attraction at pH 5.0–6.0. Meanwhile, *in situ* formed MnO_2 can also oxidize BPA efficiently under acidic pH conditions. Moreover, this study revealed the overlooked role of radical cross-coupling and complexation of redox-mediator with BPA in permanganate oxidation.

This finding provides new insight into the interaction between BPA and RMs in the Mn(VII)/RMs systems. Further work should focus on the regulation and optimization of complexation sites to obtain a complex with a highly uneven distribution of electron clouds between RM and organic contaminants, making the complex more active and easily decomposed by the oxidizers. These interactions between RMs and organic contaminants are closer to the scenario in the real water solution since the concentration of organic contaminants is much lower than that of RMs. However, in the real application, redundant RMs may result in excessive consumption of oxidizers and the underestimation of the concentration of organic contaminants due to complexation. Thus, in practical water treatment, RM dosages should be kept lower than those of Mn(VII) or other oxidizers. Additionally, cross-coupling products may be more toxic than BPA, necessitating careful regulation of redox mediator quantities.

CRediT authorship contribution statement

Honglong Zhang: Conceptualization, Data Curation, Investigation, Methodology, Writing - Original Draft, Writing - Review & Editing. **Qiaoqiao Zhao:** Software, Validation, Visualization. **Kangbao Zhong:** Software, Visualization. **Ruopeng Bai:** Software, Supervision, Validation, Visualization. **Jiaojiao Dong:** Data Curation. **Jun Ma:** Project Administration, Supervision. **Jing Zhang:** Conceptualization, Funding Acquisition, Supervision, Writing - Original Draft, Writing - Review & Editing. **Timothy J. Strathmann:** Supervision, Writing - Original Draft.

Declaration of competing interest

The authors declare that they have no known competing financial interests or personal relationships that could have appeared to influence the work reported in this paper.

Acknowledgment

This work was supported by the National Natural Science Foundations of China (No. 22076016).

Appendix A. Supplementary data

Supplementary data to this article can be found online at https://doi.org/10.1016/j.ese.2024.100421.

References

[1] M.A. La Merrill, L.N. Vandenberg, M.T. Smith, W. Goodson, P. Browne, H.B. Patisaul, K.Z. Guyton, A. Kortenkamp, V.J. Cogliano, T.J. Woodruff, L. Rieswijk, H. Sone, K.S. Korach, A.C. Gore, L. Zeise, R.T. Zoeller, Consensus on the key characteristics of endocrine-disrupting chemicals as a basis for hazard identification, Nat. Rev. Endocrinol. 16 (1) (2020) 45–57.
[2] J. Ding, L. Bu, B. Cui, G. Zhao, Q. Gao, L. Wei, Q. Zhao, D.D. Dionysiou, Assessment of solar-assisted electrooxidation of bisphenol AF and bisphenol A on boron-doped diamond electrodes, Environ. Sci. Ecotechnology 3 (2020) 100036.
[3] R. Li, S. Liu, W. Qiu, F. Yang, Y. Zheng, Y. Xiong, G. Li, C. Zheng, Transcriptomic analysis of bisphenol AF on early growth and development of zebrafish (Danio rerio) larvae, Environ. Sci. Ecotechnology 4 (2020) 100054.
[4] D. Jiang, W.-Q. Chen, X. Zeng, L. Tang, Dynamic stocks and flows analysis of bisphenol A (BPA) in China: 2000–2014, Environ. Sci. Technol. 52 (6) (2018) 3706–3715.
[5] J. Li, J. He, M.T. Aziz, X. Song, Y. Zhang, Z. Niu, Iodide promotes bisphenol A (BPA) halogenation during chlorination: evidence from 30 X-BPAs (X = Cl, Br, and I), J. Hazard Mater. 414 (2021) 125461.
[6] A. Cai, J. Deng, X. Ling, C. Ye, H. Sun, Y. Deng, S. Zhou, X. Li, Degradation of bisphenol A by UV/persulfate process in the presence of bromide: role of reactive bromine, Water Res. 215 (2022) 118288.
[7] P. Loganathan, S. Vigneswaran, J. Kandasamy, T.V. Nguyen, A. Katarzyna Cuprys, H. Ratnaweera, Bisphenols in water: occurrence, effects, and mitigation strategies, Chemosphere 328 (2023) 138560.
[8] F.J. Krembs, R.L. Siegrist, M.L. Crimi, R.F. Furrer, B.G. Petri, ISCO for groundwater remediation: analysis of field applications and performance, Groundwater Monit. Remediat. 30 (4) (2010) 42–53.
[9] A. Tsitonaki, B. Petri, M. Crimi, H. MosbÆK, R.L. Siegrist, P.L. Bjerg, In situ chemical oxidation of contaminated soil and groundwater using persulfate: a review, Crit. Rev. Environ. Sci. Technol. 40 (1) (2010) 55–91.
[10] R.H. Waldemer, P.G. Tratnyek, Kinetics of contaminant degradation by permanganate, Environ. Sci. Technol. 40 (3) (2006) 1055–1061.
[11] Z. Shi, C. Jin, R. Bai, Z. Gao, J. Zhang, L. Zhu, Z. Zhao, T.J. Strathmann, Enhanced transformation of emerging contaminants by permanganate in the presence of redox mediators, Environ. Sci. Technol. 54 (3) (2020) 1909–1919.
[12] L. Hu, H.M. Martin, T.J. Strathmann, Oxidation kinetics of antibiotics during water treatment with potassium permanganate, Environ. Sci. Technol. 44 (16) (2010) 6416–6422.
[13] H. Zhang, Z. Shi, R. Bai, D. Wang, F. Cui, J. Zhang, T.J. Strathmann, Role of TEMPO in enhancing permanganate oxidation toward organic contaminants, Environ. Sci. Technol. 55 (11) (2021) 7681–7689.
[14] M. Li, L. Fu, L. Deng, Y. Hu, Y. Yuan, C. Wu, A tailored and rapid approach for ozonation catalyst design, Environ. Sci. Ecotechnology 15 (2023) 100244.

[15] H. Zhang, Z. Shi, F. Cui, J. Zhang, T.J. Strathmann, Contribution of different reactive species in the oxidation of bisphenol A by permanganate combined with 1-hydroxybenzotriazole, Chem. Eng. J. 451 (2023) 138813.
[16] H. Zhang, Z. Shi, J. Ma, F. Cui, J. Zhang, T.J. Strathmann, Abatement of organic contaminants by Mn(VII)/TEMPOs: effects of TEMPOs structure, organic contaminant speciation, and active oxidizing species, Environ. Sci. Technol. 56 (14) (2022) 10361–10371.
[17] H. Zhang, J. Ma, J. Zhang, T.J. Strathmann, ABNO-functionalized silica as an efficient catalyst for enhancing permanganate oxidation of emerging contaminants, Environ. Sci. Technol. 57 (1) (2023) 635–642.
[18] L. Zhao, J. Zhang, J. Ma, PTIO as a redox mediator to enhance organic contaminants oxidation by permanganate, Water Res. 244 (2023) 120500.
[19] M. Deborde, S. Rabouan, P. Mazellier, J.-P. Duguet, B. Legube, Oxidation of bisphenol A by ozone in aqueous solution, Water Res. 42 (16) (2008) 4299–4308.
[20] C. Li, X.Z. Li, N. Graham, N.Y. Gao, The aqueous degradation of bisphenol A and steroid estrogens by ferrate, Water Res. 42 (1) (2008) 109–120.
[21] J. Zhang, B. Sun, X. Guan, Oxidative removal of bisphenol A by permanganate: kinetics, pathways and influences of co-existing chemicals, Sep. Purif. Technol. 107 (2013) 48–53.
[22] J. Zhang, X. Guan, Ru(III)-catalyzed permanganate oxidation of bisphenol A, Desalination Water Treat. 52 (22–24) (2014) 4592–4601.
[23] F.-D. Zhu, K.-H. Choo, H.-S. Chang, B. Lee, Interaction of bisphenol A with dissolved organic matter in extractive and adsorptive removal processes, Chemosphere 87 (8) (2012) 857–864.
[24] L.-h. Gan, Z.-r. Yan, Y.-f. Ma, Y.-y. Zhu, X.-y. Li, J. Xu, W. Zhang, pH dependence of the binding interactions between humic acids and bisphenol A - A thermodynamic perspective, Environ. Pollut. 255 (2019) 113292.
[25] Y. Wang, P. Zhang, L. Lyu, T. Li, C. Hu, Preferential destruction of micropollutants in water through a self-purification process with dissolved organic carbon polar complexation, Environ. Sci. Technol. 56 (15) (2022) 10849–10856.
[26] M. Rafiee, B. Karimi, S. Alizadeh, Mechanistic study of the electrocatalytic oxidation of alcohols by TEMPO and NHPI, Chemelectrochem 1 (2) (2014) 455–462.
[27] M. Bhardwaj, P. Grover, B. Rasool, D. Mukherjee, Recent advances in N-hyrdoxypthalimide: as a free radical initiator and its applications, Asian J. Org. Chem. 11 (11) (2022) e202200442.
[28] M. Caruso, S. Navalón, M. Cametti, A. Dhakshinamoorthy, C. Punta, H. García, Challenges and opportunities for N-hydroxyphthalimide supported over heterogeneous solids for aerobic oxidations, Coord. Chem. Rev. 486 (2023) 215141.
[29] 16 Gaussian, A.03 Revision, M.J. Frisch, G.W. Trucks, H.B. Schlegel, G.E. Scuseria, M.A. Robb, J.R. Cheeseman, G. Scalmani, V. Barone, G.A. Petersson, H. Nakatsuji, X. Li, M. Caricato, A.V. Marenich, J. Bloino, B.G. Janesko, R. Gomperts, B. Mennucci, H.P. Hratchian, J.V. Ortiz, A.F. Izmaylov, J.L. Sonnenberg, D. Williams-Young, F. Ding, F. Lipparini, F. Egidi, J. Goings, B. Peng, A. Petrone, T. Henderson, D. Ranasinghe, V.G. Zakrzewski, J. Gao, N. Rega, G. Zheng, W. Liang, M. Hada, M. Ehara, K. Toyota, R. Fukuda, J. Hasegawa, M. Ishida, T. Nakajima, Y. Honda, O. Kitao, H. Nakai, T. Vreven, K. Throssell, J.A. Montgomery Jr., J.E. Peralta, F. Ogliaro, M.J. Bearpark, J.J. Heyd, E.N. Brothers, K.N. Kudin, V.N. Staroverov, T.A. Keith, R. Kobayashi, J. Normand, K. Raghavachari, A.P. Rendell, J.C. Burant, S.S. Iyengar, J. Tomasi, M. Cossi, J.M. Millam, M. Klene, C. Adamo, R. Cammi, J.W. Ochterski, R.L. Martin, K. Morokuma, O. Farkas, J.B. Foresman, D.J. Fox, Gaussian, Inc., Wallingford CT, 2016.
[30] A.D. Becke, Density-functional thermochemistry. III. The role of exact exchange, J. Chem. Phys. 98 (7) (1993) 5648–5652.
[31] S. Grimme, S. Ehrlich, L. Goerigk, Effect of the damping function in dispersion corrected density functional theory, J. Comput. Chem. 32 (7) (2011) 1456–1465.
[32] A.V. Marenich, C.J. Cramer, D.G. Truhlar, Universal solvation model based on solute electron density and on a continuum model of the solvent defined by the bulk dielectric constant and atomic surface tensions, J. Phys. Chem. B 113 (18) (2009) 6378–6396.
[33] W. Humphrey, A. Dalke, K. Schulten, VMD: visual molecular dynamics, J. Mol. Graph. 14 (1) (1996) 33–38.
[34] T. Lu, F. Chen Multiwfn, A multifunctional wavefunction analyzer, J. Comput. Chem. 33 (5) (2012) 580–592.
[35] Q. Luo, Z. Wang, M. Feng, D. Chiang, D. Woodward, S. Liang, J. Lu, Q. Huang, Factors controlling the rate of perfluorooctanoic acid degradation in laccase-mediator systems: the impact of metal ions, Environ. Pollut. 224 (2017) 649–657.
[36] J. Jiang, S.-Y. Pang, J. Ma, Oxidation of triclosan by permanganate (Mn(VII)): importance of ligands and in situ formed manganese oxides, Environ. Sci. Technol. 43 (21) (2009) 8326–8331.
[37] J. Jiang, S.-Y. Pang, J. Ma, Role of ligands in permanganate oxidation of organics, Environ. Sci. Technol. 44 (11) (2010) 4270–4275.
[38] F. Freeman, J.C. Kappos, Permanganate ion oxidations. 15. Additional evidence for formation of soluble (colloidal) manganese dioxide during the permanganate ion oxidation of carbon-carbon double bonds in phosphate-buffered solutions, J. Am. Chem. Soc. 107 (23) (1985) 6628–6633.
[39] B. Sun, J. Zhang, J. Du, J. Qiao, X. Guan, Reinvestigation of the role of humic acid in the oxidation of phenols by permanganate, Environ. Sci. Technol. 47 (24) (2013) 14332–14340.
[40] B. Sun, Mechanism Investigation of the Influence of Humic Acid on Phenol Oxidation by Permanganate, Harbin Institute of Technology, Harbin, 2013. Master.
[41] Y. Song, J. Jiang, J. Ma, S.-Y. Pang, Y.-z. Liu, Y. Yang, C.-w. Luo, J.-q. Zhang, J. Gu, W. Qin, ABTS as an electron shuttle to enhance the oxidation kinetics of substituted phenols by aqueous permanganate, Environ. Sci. Technol. 49 (19) (2015) 11764–11771.
[42] K. Xu, W. Ben, W. Ling, Y. Zhang, J. Qu, Z. Qiang, Impact of humic acid on the degradation of levofloxacin by aqueous permanganate: kinetics and mechanism, Water Res. 123 (2017) 67–74.
[43] Z. Shi, C. Jin, J. Zhang, L. Zhu, Insight into mechanism of arsanilic acid degradation in permanganate-sulfite system: role of reactive species, Chem. Eng. J. 359 (2019) 1463–1471.
[44] C. D'Alfonso, M. Bietti, G.A. DiLabio, O. Lanzalunga, M. Salamone, Reactions of the phthalimide *N*-oxyl radical (PINO) with activated phenols: the contribution of π-stacking interactions to hydrogen atom transfer rates, J. Org. Chem. 78 (3) (2013) 1026–1037.
[45] J.E. Nutting, M. Rafiee, S.S. Stahl, Tetramethylpiperidine *N*-oxyl (TEMPO), phthalimide *N*-oxyl (PINO), and related *N*-oxyl species: electrochemical properties and their use in electrocatalytic reactions, Chem. Rev. 118 (9) (2018) 4834–4885.
[46] S. Coseri, Phthalimide-*N*-oxyl (PINO) radical, a powerful catalytic agent: its generation and versatility towards various organic substrates, Catal. Rev. 51 (2) (2009) 218–292.
[47] N. Koshino, B. Saha, J.H. Espenson, Kinetic study of the phthalimide *N*-oxyl radical in acetic acid. Hydrogen abstraction from substituted toluenes, benzaldehydes, and benzyl alcohols, J. Org. Chem. 68 (24) (2003) 9364–9370.
[48] S. Duan, H. Dong, P. Hou, G. Han, B. Zhang, Z. Qiang, Simultaneous oxidation of trace organic contaminant and Mn(II) by Mn(VII): accelerating role of dissolved oxygen, Chemosphere 308 (2022) 136321.
[49] J.E. Tobiason, A. Bazilio, J. Goodwill, X. Mai, C. Nguyen, Manganese removal from drinking water sources, Curr. Pollut. Rep. 2 (3) (2016) 168–177.
[50] K. Lin, W. Liu, J. Gan, Oxidative removal of bisphenol A by manganese dioxide: efficacy, products, and pathways, Environ. Sci. Technol. 43 (10) (2009) 3860–3864.
[51] J. Luo, J. Zhang, Aerobic oxidation of olefins and lignin model compounds using photogenerated phthalimide-*N*-oxyl radical, J. Org. Chem. 81 (19) (2016) 9131–9137.
[52] R.-Z. Xu, J.-S. Cao, G. Feng, J.-Y. Luo, Q. Feng, B.-J. Ni, F. Fang, Fast identification of fluorescent components in three-dimensional excitation-emission matrix fluorescence spectra via deep learning, Chem. Eng. J. 430 (2022) 132893.
[53] L. Li, Y. Wang, W. Zhang, S. Yu, X. Wang, N. Gao, New advances in fluorescence excitation-emission matrix spectroscopy for the characterization of dissolved organic matter in drinking water treatment: a review, Chem. Eng. J. 381 (2020) 122676.